J. Fluid Mech. (2003), *vol.* 478, *pp.* 135–163.
DOI: 10.1017/S0022112002003348 Printed in the United Kingdom

Three-dimensional acoustic-roughness receptivity of a boundary layer on an airfoil: experiment and direct numerical simulations

By W. WÜRZ[1], S. HERR[1], A. WÖRNER[1], U. RIST[1], S. WAGNER[1] AND Y. S. KACHANOV[2]

[1]Institut für Aerodynamik und Gasdynamik, Universität Stuttgart, Pfaffenwaldring 21, 70550 Stuttgart, Germany

[2]Institute of Theoretical and Applied Mechanics, Institutskaya str. 4/1, Novosibirsk, 630090, Russia

(Received 28 January 2002 and in revised form 28 August 2002)

The paper is devoted to an experimental and numerical investigation of the problem of excitation of three-dimensional Tollmien–Schlichting (TS) waves in a boundary layer on an airfoil owing to scattering of an acoustic wave on localized microscopic surface non-uniformities. The experiments were performed at controlled disturbance conditions on a symmetric airfoil section at zero angle of attack. In each set of measurements, the acoustic wave had a fixed frequency f_{ac}, in the range of unstable TS-waves. The three-dimensional surface non-uniformity was positioned close to the neutral stability point at branch I for the two-dimensional perturbations. To avoid experimental difficulties in the distinction of the hot-wire signals measured at the same (acoustic) frequency but having a different physical nature, the surface roughness was simulated by a quasi-stationary surface non-uniformity (a vibrator) oscillating with a low frequency f_v. This led to the generation of TS-wavetrains at combination frequencies $f_{1,2} = f_{ac} \mp f_v$. The spatial behaviour of these wavetrains has been studied in detail for three different values of the acoustic frequency. The disturbances were decomposed into normal oblique TS-modes. The initial amplitudes and phases of these modes (i.e. at the position of the vibrator) were determined by means of an upstream extrapolation of the experimental data. The shape of the vibrator oscillations was measured by means of a laser triangulation device and mapped onto the Fourier space.

The direct numerical simulations (DNS) are based on the vorticity–velocity formulation of the complete Navier–Stokes equations using a uniformly spaced grid in the streamwise and wall-normal direction and a spectral representation in the spanwise direction. For the present investigation, the sound wave in the free stream is prescribed as a solution of the second Stokes' problem at inflow, and a novel wall model has been implemented. The three-dimensional simulations were performed for a stationary surface non-uniformity.

As a result of the present study, the acoustic receptivity coefficients are obtained both in experiment and DNS as functions of the spanwise wavenumber and acoustic frequency. The receptivity amplitudes and phases obtained numerically are in very good agreement with those obtained experimentally in the studied range of parameters. The scattering of acoustic waves on three-dimensional surface non-uniformities is found to be significantly stronger than that on two-dimensional surface non-uniformities. The obtained data are independent of the specific shape of the surface

non-uniformity and can be used for estimation of the initial amplitudes of the three-dimensional TS-waves, as well as for the validation of other three-dimensional receptivity theories.

1. Introduction

For many years, the problem of boundary-layer transition from the laminar to the turbulent state has attracted great attention because of its fundamental and practical importance. This problem includes three main aspects: (i) the receptivity of the laminar flow to external perturbations, (ii) the linear development of small-amplitude boundary-layer instabilities, and (iii) the nonlinear flow breakdown to turbulence.

The present paper is devoted to experimental and numerical investigations of the first of these aspects, namely the linear three-dimensional acoustic receptivity of a two-dimensional laminar boundary layer in the presence of localized (in streamwise direction) surface non-uniformities with various spanwise scales.

The receptivity of the boundary-layer flow to external perturbations represents an important aspect of the laminar–turbulent transition problem, which has both basic and practical significance. This problem was clearly formulated for the first time by Morkovin (1968). The receptivity describes mechanisms by means of which the instability waves are excited in the boundary layers under the influence of some external (with respect to the boundary-layer flow) perturbations. Starting with the classic work by Schubauer & Skramstad (1947), various methods of excitation of the boundary-layer instability modes have been used during the past fifty years in many experiments devoted to the investigation of linear and nonlinear stability problems. However, the *mechanisms* of the generation of instability waves were not studied until the 1960s. Gaster (1965) was probably the first theoretical work directly devoted to this problem. It provides a foundation for investigation of boundary-layer receptivity to localized surface disturbances.

The first detailed quantitative studies of the receptivity problem were performed in the 1970s. The experiments by Kachanov, Kozlov & Levchenko (1975, 1978) and Kachanov *et al.* (1979) were devoted to the study of the excitation of two-dimensional Tollmien-Schlichting (TS) waves in the vicinity of an elliptic flat-plate leading edge by means of free-stream vortices, acoustic waves and surface vibrations. The experimental results were compared by Kachanov *et al.* (1979) with those obtained by Maksimov (1979) in his direct numerical simulations. In particular, it was shown that free-stream vortices could excite the TS-waves effectively when they hit the plate leading edge (which represented a significant spatial non-uniformity). An important role of the normal-to-wall component of the velocity fluctuations has been shown. However, far from the plate nose the same vortices did not excite any remarkable instability waves because of much weaker streamwise flow non-uniformity. Very similar results were obtained theoretically by Rogler & Reshotko (1975), Rogler (1977) and Maksimov (1979).

Kachanov *et al.* (1975) have also found that an acoustic wave, propagating along the streamwise axis, does not directly produce any significant TS-waves on the plate leading edge, but leads to surface vibrations, which excite the instability waves in the vicinity of the attachment line. Aizin & Polyakov (1979) found in their experimental and theoretical work that the streamwise acoustic wave produces two-dimensional TS-waves very effectively during its scattering on a microscopic localized surface non-

uniformity (a strip of plastic film). The two-dimensional acoustic receptivity problem was also studied theoretically by Mangur (1977), Tam (1978), Maksimov (1979) (see also Kachanov *et al.* 1979), Murdock (1980) and others. The state-of-the-art in the field at that time was reviewed by Loehrke, Morkovin & Fejer (1975), Reshotko (1976) and Morkovin (1977). This initial period of direct studies of the receptivity problem has been summarized by Kachanov, Kozlov & Levchenko (1982) and by Leehey (1980) and Nishioka & Morkovin (1986).

Later, the receptivity problem was investigated in a large number of theoretical and experimental studies. From now on, we concentrate mainly on subsequent investigations of the *acoustic receptivity problem.*

In the 1980s–1990s, the mechanisms of generation of instability waves in two-dimensional boundary layers by means of acoustic perturbations in the presence of a localized (in the streamwise direction) surface non-uniformity, such as a roughness element, a suction slot, surface vibration and others, were studied in detail for two-dimensional disturbances. The most important theoretical results obtained in this field by the mid 1990s are discussed by Zhigulyov & Tumin (1987), Goldstein & Hultgren (1989), Kerschen (1989), Kerschen, Choudhari & Heinrich (1990), Kozlov & Ryzhov (1990), Morkovin & Reshotko (1990), Choudhari & Streett (1992), Crouch (1994) Choudhari (1994) and others. It is necessary to note some important experimental papers devoted to this problem. After the famous work by Aizin & Polyakov (1979) the excitation of the two-dimensional instability waves by acoustics on two-dimensional roughness elements was studied experimentally by Kosorygin, Levchenko & Polyakov (1985), Kosorygin (1986), Saric, Hoos & Kohama (1990), Wiegel & Wlezien (1993), Zhou, Liu & Blackwelder (1994), Kosorygin, Radeztsky & Saric (1995) and others. It was found that the acoustics excite the two-dimensional TS-waves even on a microscopically small non-uniformity. The receptivity coefficients were estimated in these studies for different acoustic frequencies, roughness shapes and acoustic wave inclination angles. A good agreement between theory and experiment was usually observed.

Choudhari & Kershen (1990) probably obtained the first theoretical results on the generation of TS-waves by acoustics on a three-dimensional surface roughness element (or localized three-dimensional suction) for a two-dimensional boundary layer. A similar problem was investigated theoretically by Tadjfar & Bodonyi (1992) with the help of non-stationary linearized three-dimensional equations for the asymptotic triple-deck model of the two-dimensional boundary layer. A qualitative comparison of these results with previous experiments by Gilyov & Kozlov (1984) and Tadjfar (1990) was also performed in this paper. The excitation of the TS-waves by acoustics on three-dimensional roughness elements, such as an oblique surface roughness strip and a circular roughness, was investigated experimentally by Zhou *et al.* (1994). Choudhari & Kerschen (1990) found these results to be in a good qualitative agreement with theory.

Similarly to two-dimensional boundary layers, the acoustic fields can represent a possible source for cross-flow (CF) instability waves in swept-wing boundary layers. As shown by Crouch (1993, 1994), the acoustic receptivity mechanism does exist and can play a role in the transition process at high enough levels of acoustic excitation. In these theoretical works, a scattering of the acoustic wave on a stationary localized surface non-uniformity (roughness) was investigated. This mechanism was found and investigated experimentally by Ivanov, Kachanov & Koptsev (1998*a*) on a model of a swept wing. In addition Ivanov, Kachanov & Koptsev (1997) studied the case of an unsteady surface non-uniformity, i.e. when it is represented by a localized surface

vibrator (oscillated with low frequency). In this case, the mechanism of excitation of the CF instability wave was quasi-stationary. The values of the acoustic receptivity coefficients were estimated in these experiments, but not compared with theory.

Cullen & Horton (1999) studied the acoustic receptivity for a stationary localized three-dimensional roughness in a two-dimensional boundary layer, but no quantitative receptivity coefficients were evaluated. For the first time, these coefficients were obtained experimentally by Würz *et al.* (1998) for a single acoustic frequency and compared with calculations in Würz *et al.* (1999). The subsequent development of these studies is discussed in the present paper.

Thus, the present study concentrates, for the first time, on a *quantitative* investigation of the three-dimensional boundary-layer acoustic receptivity, including a direct comparison of values of the experimental and numerical receptivity coefficients.

The three-dimensional acoustic receptivity problem seems to be very important owing to the following circumstances. It is well known that the transition process in two-dimensional subsonic boundary layers has an essentially three-dimensional character (see e.g. Klebanoff, Tidstrom & Sargent 1962). Nevertheless, three-dimensional instability waves in these flows were of only limited interest to investigators, probably because of the well-known Squire (1933) theorem, which is usually interpreted to mean that the two-dimensional TS-waves are the most dangerous from the viewpoint of transition. However, this interpretation is not quite correct, especially for spatially growing perturbations and in not strictly parallel flows (see experimental results by Kachanov & Obolentseva 1996, 1998 and theoretical ones by Bertolotti 1991). On the other hand, it is well known that in two-dimensional subsonic boundary layers the three-dimensional waves also play a very significant role at nonlinear stages of transition, even if their initial amplitudes are small. These three-dimensional perturbations participate in the resonant interactions with primary waves and become dominant at certain stages of transition (see e.g. Kachanov & Levchenko 1984; Saric, Kozlov & Levchenko 1984). The scenarios and the position of transition strongly depend on the initial amplitudes and phases of these three-dimensional disturbances, which in turn depend on the three-dimensional receptivity mechanisms.

A significant methodological foundation for the study described in the present paper was made in a set of previous theoretical and experimental studies. The notions associated with the localized linear receptivity coefficients for the normal instability modes of the frequency–wavenumber spectrum were developed in theoretical investigations by Gaster (1965), Terent'ev (1981), Zavol'skii, Reutov & Rybushkina (1983), Ruban (1985), Goldstein (1985), Fyodorov (1988), Choudhari & Kerschen (1990), Crouch (1992) and others. The methods of experimental determination of the three-dimensional receptivity coefficients for normal modes were developed by Gaponenko, Ivanov & Kachanov (1996), Ivanov *et al.* (1997, 1998*a*,*b*), Bake *et al.* (2001) and others. (A review of these and other recent studies of the three-dimensional receptivity problem can be found in Kachanov 2000.)

2. Experimental procedure and definition of receptivity functions

2.1. *Wind-tunnel, experimental model and basic-flow characteristics*

The experiments were carried out in the Laminar Wind Tunnel (figure 1) of the 'Institut für Aerodynamik und Gasdynamik (IAG)' (Wortmann & Althaus 1964). The Laminar Wind Tunnel is an open return tunnel with a closed test section. The rectangular test section has a cross-section of $0.73 \times 2.73\,\mathrm{m}^2$ and a length of 3.15 m. A two-dimensional airfoil model spans the short distance of the test section. The high

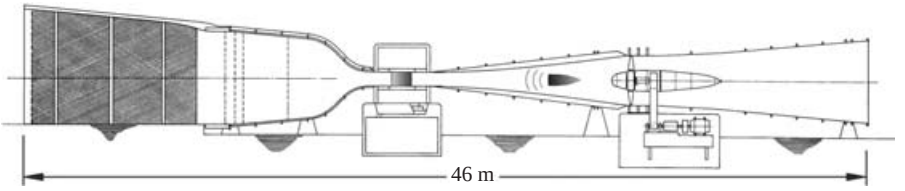

FIGURE 1. The Laminar Wind Tunnel of the IAG.

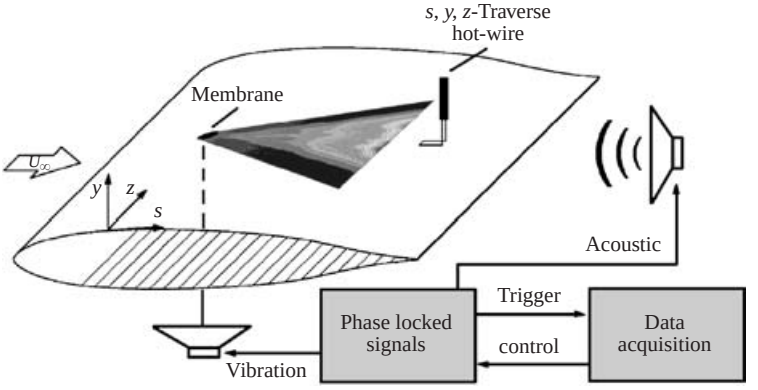

FIGURE 2. Sketch of the experimental set-up.

contraction ratio of 100 : 1 and the system of screens and filters result in a very low turbulence level of less than $Tu = \sqrt{\overline{u'^2}}/U_\infty = 2 \times 10^{-4}$ for a frequency range of 20–5000 Hz and a flow velocity of 30 m s^{-1}. Above 200 Hz, the measured free-stream velocity fluctuations are in the range of the electronic noise of standard hot-wire equipment.

The experimental set-up is shown in figure 2. The receptivity measurements were performed on an airfoil section 'XIS40MOD' (Würz 1995) with 15% thickness, which was specially designed to have a long instability ramp at zero angle of attack and different flow regimes can be established by changing this angle. The airfoil was manufactured from reinforced fibreglass in a numerically controlled milled mould. Remaining roughness r.m.s. heights of the model surface are in the order of 0.5 μm measured with a precision surface measuring system.

The free-stream velocity was chosen to be $U_\infty = 30\,\mathrm{m\,s^{-1}}$. This results in a Reynolds number of $Re \approx 1.23 \times 10^6$ based on the arclength $s_{max} = 0.615$ m of the airfoil measured from the leading edge and the averaged kinematic viscosity $\nu = 15 \times 10^{-6}\,\mathrm{m^2\,s^{-1}}$. Taking into account the quadratic influence of the free-stream velocity on the non-dimensional frequency parameter $F = 2\pi f \nu / U_\delta^2$ (where U_δ is the local free-stream velocity), the velocity was fixed instead of the Reynolds number.

The basic pressure distribution was evaluated from the readings of 48 pressure orifices, with the boundary-layer traversing mechanism placed at the measurement position chosen to take its influence into account. The measured values were compared with distributions calculated from XFOIL (see e.g. Drela & Giles 1986) for a series of slightly different angles of attack until they gave the best fit to the experimental data. This distribution (figure 3) was then used for the calculation of boundary-layer profiles with a finite-difference scheme according to Cebeci & Smith (1974). Because of the long instability ramp, the shape factor $H_{12} = \delta_1/\delta_2$ increases nearly linearly from

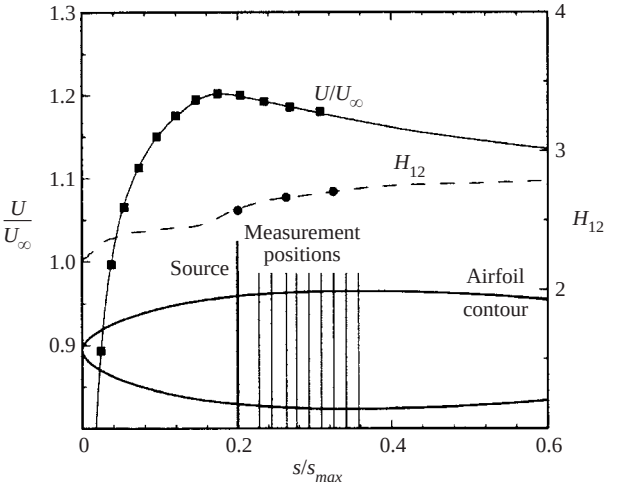

FIGURE 3. —, Calculated velocity distribution and - - -, development of the shape factor H_{12}, together with the airfoil contour and the positions of measurement. Symbols denote measured values.

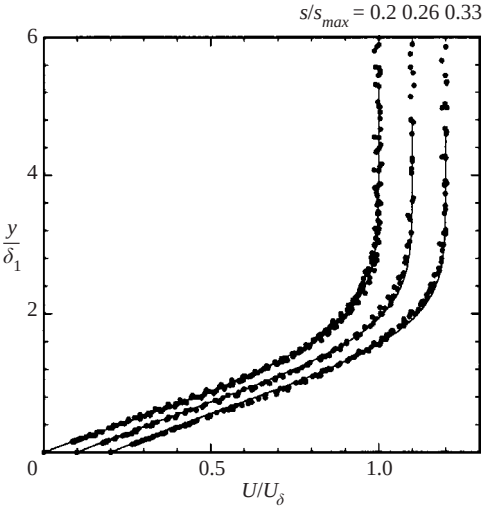

FIGURE 4. Mean velocity profiles for different streamwise positions. Profiles shifted by $\Delta(U/U_\delta) = 0.1$. Lines are boundary-layer calculation.

the value $H_{12} = 2.58$ at $s/s_{max} = 0.2$ to $H_{12} = 2.71$ at the end of the measurement region at $s/s_{max} = 0.33$ (δ_1 and δ_2 are the boundary-layer displacement thickness, momentum thickness, respectively).

Mean flow velocity profiles were measured at three downstream positions and are presented in figure 4 (symbols) together with the calculated ones (lines), which fit quite well to the experimental data. The shape factor $H_{12} = 2.58$, measured at the position of the surface non-uniformity ($s/s_{max} = 0.2$), is very close to the Blasius value of $H_{12} = 2.59$. Nevertheless, owing to prehistory effects of the boundary layer, the shape of the profile can show in detail some deviations from the Blasius profile.

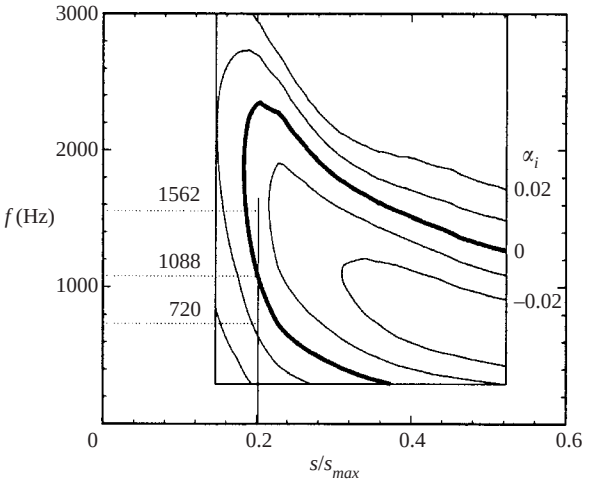

FIGURE 5. Stability diagram for two-dimensional TS-waves. Position of the vibrator at $0.2\,s/s_{max}$. The investigated frequencies are marked by dotted lines. ($U_\delta(s/s_{max} = 0.2) = 36\,\mathrm{m\,s^{-1}}$, $\nu = 15 \times 10^{-6}\,\mathrm{m^2\,s^{-1}}$.

Despite this fact, stability calculations for the present configuration showed that these deviations are negligible.

The displacement thickness, $\delta_{1ref} = 0.36\,\mathrm{mm}$, at the position of the surface non-uniformity was used to normalize all length scales in this paper, whereas the velocities (and the amplitudes of its fluctuations) were always normalized by the local free-stream speed.

2.2. *Generation of controlled disturbances*

Two kinds of disturbance were produced in the experiments: (i) the acoustic wave and (ii) the surface non-uniformity. The acoustic wave was generated by a 1020 McCauley loudspeaker located at the wind-tunnel axis about 4.4 m downstream of the test section and propagated upstream. The sound pressure level was of the order of 100 dB. Three fixed frequencies were investigated: $f_{ac} = 720, 1088$ and $1562\,\mathrm{Hz}$. As the local free-stream velocity at the position of the surface non-uniformity was kept at $U_\delta = 36\,\mathrm{m\,s^{-1}}$, these fixed frequencies correspond at this position to the non-dimensional frequency parameters $F \times 10^6 = 52.4,\ 79.1$ and 113.6, respectively. In the streamwise region of the main measurements, these frequencies lie in the range of unstable TS-modes, as is seen in figure 5. The stability diagram shown in this figure (for two-dimensional waves) was calculated with a shooting solver (Conte 1966) for the solution of the Orr–Sommerfeld equation.

The surface non-uniformity was designed based on the following circumstances. When studying the three-dimensional acoustic-roughness receptivity, the data analysis represents a very complicated problem because of difficulties in distinguishing signals measured at the same (acoustic) frequency but having different physical natures (i) the instability wave generated by the acoustics (which is relatively weak initially), (ii) vibrations of the hot-wire probe and the model surface, and (iii) the acoustic field itself, including the Stokes layer in the near-wall region. These experimental problems have been solved by Ivanov *et al.* (1997). A similar method has been applied in the present investigation. The surface non-uniformity was simulated by a quasi-steady (low-frequency) localized surface vibrator driven at frequency $f_v = \frac{1}{64} f_{ac}$. This led to

the generation of TS-wavetrains at combination frequencies $f_{1,2} = f_{ac} \mp f_v$, which corresponded *only* to the instability waves generated due to a scattering of the acoustic wave on the quasi-steady roughness. The disturbances at these combination frequencies, detuned from the frequency of the acoustics (and vibrations), can be measured relatively easily. The spatial behaviour of these combination modes has been studied in detail.

The position of the surface vibrator ($s/s_{max} = 0.2$, $Re_{\delta 1} = 805$) was selected close to the first branch of the two-dimensional neutral stability curve for the middle frequency of 1088 Hz (see figure 5). The vibrator had a diameter of $d = 6$ mm. Its vinyl membrane, driven by pressure fluctuations produced by a loudspeaker, was mounted flush with the model surface. To avoid a steady deflection of the membrane, the static pressure of this pneumatic system was established by a static pressure orifice positioned on the airfoil surface at the same streamwise station as the vibrator. The shape of the membrane oscillation was measured in 600 points in the (s, z)-plane with a Micro-Epsilon LD1605-0.5 laser triangulation device with a specified linearity below $\pm 0.2\%$ for a range of ± 0.25 mm.

During the main measurements, the maximum vibrational r.m.s. amplitude A_v was rather low (29.7 μm) in order to be in the linear regime of the receptivity and to have a linear behaviour of the boundary-layer instability waves (see §§ 4 and 5 for more details). The equivalent non-dimensional roughness height $h_r = A_v/\delta_1 = 0.083$ is therefore well below the value of $h_r = 0.17$ for which Saric, Hoos & Radeztsky (1991) found the first nonlinear response for two-dimensional roughness elements and an acoustic forcing of 100 dB.

2.3. *Procedures of measurements and data acquisition*

The main measurements have been performed by a hot-wire anemometer. A modified DISA 55P15 boundary-layer probe with wire of 1 mm in length was used together with a DISA 55M10 bridge. The calibration of the hot wire was made according to Kings law and the coefficients were optimized for minimum standard deviation. A small static pressure probe was used during measurements as a velocity reference at the boundary-layer edge. The probes were mounted on a traversing system, which allows computer controlled scans in the wall-normal direction with an accuracy of 5 μm and scans in the spanwise direction with an accuracy of 0.1 mm.

The d.c.-output of the hot-wire anemometer was integrated with a 1 Hz low-pass filter. The a.c.-output was high-pass filtered with a first-order low-noise filter with a cutoff frequency of 100 Hz (for $f_{ac} = 1088$ Hz and $f_{ac} = 1562$ Hz) and 55 Hz (for $f_{ac} = 720$ Hz). A programmable amplifier (amplification factor 1 to 3999) was used to fit the signal always optimally to the input range of the 12 bit AD-converter. Prior to sampling, the signal was additionally low-pass filtered (fourth-order) at 4400 Hz to omit aliasing problems. The acoustic and vibrational frequency, as well as the digital sampling trigger, were generated strictly phase locked by a single quartz-based clock (figure 2). The ratios between the frequencies were chosen as integer powers of two ($f_v : f_{ac} : f_{sample} = 1 : 64 : 8$), therefore they could be represented with a single Fourier series coefficient after one fast Fourier transform. After establishment of the sound field and the TS-wavetrain, five sets of 4096 points were collected and ensemble averaged in the time domain. The fast Fourier transform analysis was performed and the Fourier coefficients were corrected in amplitude and phase for the influence of the filters. All results were monitored on-line.

To account for small possible drifts in the acoustic and vibrational amplitude, two reference points were defined. The amplitude and phase of the acoustic wave

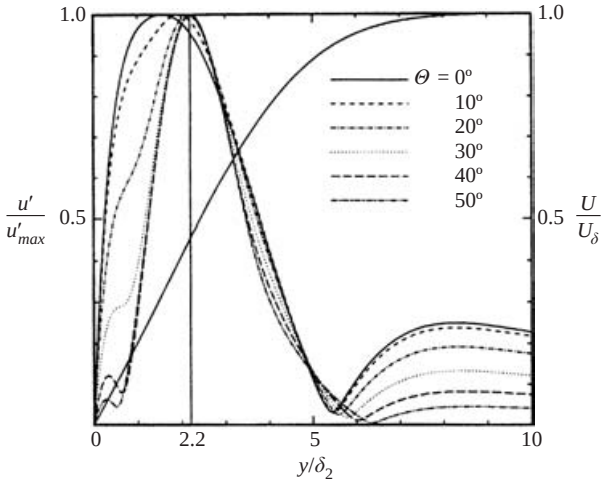

FIGURE 6. Mean velocity profile and calculated TS-eigenfunctions for different propagation angles. Linear stability theory for 1088 Hz and the position $s/s_{max} = 0.263$.

were measured before and after every spanwise scan by positioning the hot wire at the s-position of the vibrator, but with 20 mm offset in the spanwise direction and outside the Stokes layer and the boundary layer. To control the vibrational amplitude and phase, the hot wire was positioned at a reference point over the vibrator and just outside the boundary layer; the velocity fluctuations measured at this point are in phase with the surface vibrations. At the start and the end of every main set of measurements, the amplitude of the membrane deflection was measured with the laser triangulation device, which gave a fixed relationship between the velocity fluctuations and the surface displacement at the frequency of the vibration.

The initial amplitudes of the excited TS-waves, which are necessary for determining the receptivity coefficients (see § 2.4), cannot be measured directly in the flow because in the near field of the vibrator a mixture of different other perturbations, such as continuous-spectrum instability modes and forced (bounded) fluctuations, is present. Therefore, a main set of the boundary-layer measurements consisted of 8 or 9 spanwise distributions of the TS amplitudes and phases measured *downstream* of the surface non-uniformity at chordwise positions s_i corresponding to the linear stage of the disturbance development (see figure 3). Then, the spectral amplitudes and phases were extrapolated back to the position of the centre of the surface non-uniformity (see § 5 for more details). The first measurement station s_1, located approximately two TS-wavelengths downstream of the vibrator, was found to be outside the near field. The amplitudes at the combination frequencies $f_{1,2}$ were corrected according to the acoustic and vibrational amplitudes measured in the reference points described above. A similar correction was also applied to the TS-wave phases. The resulting phases were 'normalized' by the acoustic phase, i.e. the acoustic phase was subtracted from the phases of the TS-waves.

For the spanwise scans, a certain wall-normal distance had to be chosen, which should be close to the amplitude maxima of normal two-dimensional and three-dimensional TS-waves in their eigenfunctions. The calculations (figure 6) show that these maxima do not coincide completely, but a good compromise is given for $y/\delta_2 = 2.2$, especially for $f_{ac} = 720$ Hz and 1088 Hz (see also discussion in § 7.1). This

position was adjusted during the measurements of spanwise scans by keeping U/U_δ constant at the necessary corresponding value.

In order to obtain the receptivity phases for the case $f_v \to 0$, which would be interpreted correctly in terms of the acoustic wave scattering on a frozen vibrator (i.e. on an equivalent roughness), it was necessary to choose correctly the origin of the time axis. This origin has to be chosen at the time moment when the phase of the membrane oscillations is equal to zero (for the cosine wave). In this case, we have, at $f_v = 0$, the vibrator frozen at the position of its maximum positive deviation (i.e. a steady hump) and the phases of the combination modes at frequencies $f_{1,2}$ are equal to each other. When $f_v \to 0$ these two modes collapse to one frequency mode with $f = f_{ac}$, the phase of which is the same as that for the steady roughness. The corresponding shift of the time-axis origin was made during data processing. Simultaneously, the signal phases were corrected to take into account the frequency-dependent phase shift of the filters used for signal conditioning.

2.4. *Definition of receptivity functions*

In general, the amplitude of the acoustic receptivity coefficient can be defined as the ratio of complex amplitudes of the initial instability wave amplitude, to those of the external acoustic perturbation and the involved surface non-uniformity (see Choudhari & Streett 1992; Crouch 1993; Ivanov *et al.* 1997). More exactly, all these complex amplitudes must be determined for every single (normal) mode of the corresponding frequency–wavenumber spectra.

At the conditions of the present experiment, the acoustic wave has a very large streamwise wavelength (about 330 mm) compared to the streamwise size of the surface non-uniformity (6 mm). In this case, the acoustic-wave streamwise wavenumber α_{ac} can be regarded as equal to zero. As the spanwise wavenumber of the two-dimensional acoustic wave β_{ac} is also equal to zero in this study, the acoustic wave itself can be conceded as just a harmonic in time oscillation of the free stream. The same is true for the DNS performed for incompressible fluid. Because of this, the acoustic receptivity coefficients (functions) are defined in the present paper in the following way.

In the experiment, the acoustic-vibration receptivity coefficient is

$$\bar{G}_{av}(f_{1,2}, \beta) = G_{av}(f_{1,2}, \beta)\exp(\mathrm{i}\phi_{av}(f_{1,2}, \beta)) := \frac{\bar{B}_{inTS}(f_{1,2}, \beta)}{\bar{A}_{ac}(f_{ac})\tilde{\bar{C}}_v(f_{1,2}, \tilde{\alpha}_{r1,2}, \beta)}, \tag{2.1}$$

where

$$\tilde{\alpha}_{r1,2} = \tilde{\alpha}_r(f_{1,2}, \beta) \tag{2.2}$$

is the dispersion relationship for the corresponding three-dimensional TS-waves determined at the streamwise position of the surface vibrator. Here,

$$\bar{B}_{inTS}(f_{1,2}, \beta) = B_{inTS}(f_{1,2}, \beta)\exp(\mathrm{i}\phi_{inTS}(f_{1,2}, \beta)) \tag{2.3}$$

is the initial (i.e. at the centre of the vibrator) complex spectrum of the excited TS-waves,

$$\bar{A}_{ac} = A_{ac}\exp(\mathrm{i}\varphi_{ac}) \tag{2.4}$$

is the complex amplitude of the acoustic wave over the centre of the vibrator, and

$$\tilde{\bar{C}}_v(f_{1,2}, \tilde{\alpha}_{r1,2}, \beta) = \tilde{C}_v(f_{1,2}, \tilde{\alpha}_{r1,2}, \beta)\exp(\mathrm{i}\tilde{\lambda}_v(f_{1,2}, \tilde{\alpha}_{r1,2}, \beta)) \tag{2.5}$$

is the two-dimensional complex resonant spectrum of the shape of vibrations. All functions and variables with an overbar are complex, whereas those without a bar are real. B_{inTS}, A_{ac} and $\tilde{C}_v$ are the corresponding real amplitudes and ϕ_{inTS}, φ_{ac} and

$\tilde{\lambda}_v$ are the corresponding real phases. A tilde designates the resonant parts of the two-dimensional spectrum of the surface non-uniformity, i.e. those spectral components, which correspond to the dispersion relationship (2.2). Note that the two-dimensional spectrum of vibrations

$$\bar{C}_v(\alpha_r, \beta) = C_v(\alpha_r, \beta)\exp(\mathrm{i}\lambda_v(\alpha_r, \beta)), \tag{2.6}$$

is independent of the frequency (of vibrations) as it was found experimentally (see § 2.2), whereas the resonant spectrum of vibrations, (2.5), depends on the frequency of the excited TS-wave.

The DNS are performed for the interaction of a sound wave with steady roughness. In this case, $f_1 = f_2 = f_{ac}$ and the definition (2.1) is reduced to

$$\bar{G}_{ar}(f_{ac}, \beta) = G_{ar}(f_{ac}, \beta)\exp(\mathrm{i}\phi_{ar}(f_{ac}, \beta)) := \frac{\bar{B}_{inTS}(f_{ac}, \beta)}{\bar{A}_{ac}(f_{ac})\tilde{\bar{C}}_r(f_{ac}, \tilde{\alpha}_{rac}, \beta)}, \tag{2.7}$$

where $\tilde{\alpha}_{rac} = \tilde{\alpha}_r(f_{ac}, \beta)$ is the dispersion relationship for the corresponding three-dimensional TS-wave excited at the acoustic frequency and $\tilde{\bar{C}}_r$ is the complex resonant spectrum of the roughness shape.

Definitions (2.1) and (2.7) correspond to each other when the vibrational frequency is infinitely small. This is true (in a physical sense) for the present experimental conditions. Indeed, there are three time scales, which characterize the problem: (i) the acoustic-wave period $T_{ac} = 1/f_{ac} \approx 1$ ms, (ii) the vibrational period $T_v = 1/f_v \approx 60$ ms, and (iii) the period of the passing of the basic flow over the vibrator (with diameter $d = 6$ mm) $T_b = d/U_e \approx 0.17$ ms. It is seen that, for the present experimental conditions, $T_{ac} \ll T_v$ and $T_b \ll T_v$. This means that the vibrator remains 'frozen' (it represents, in fact, a roughness element) during one period of the acoustic oscillation and during the passing of the flow over it. Therefore, in the present case, the acoustic-vibration receptivity function $\bar{G}_{av}(f_{1,2}, \beta)$ determined experimentally is equivalent to the acoustic-roughness receptivity function $\bar{G}_{ar}(f_{ac}, \beta)$ and in the final diagrams (figure 18 *a*, *b*, *c*) the subscript *ar* is used also for the experimental values.

All functions occurring on the right-hand sides of expressions (2.1) and (2.7), i.e. functions (2.3), (2.4) and (2.5), have to be found during the investigation for determining the receptivity coefficients. For determination of the resonant spectrum (2.5), the dispersion function (2.2) and the two-dimensional spectrum of vibration (2.6) also have to be found.

Further steps for the experimental evaluation of the receptivity functions are described in § 4. The results presented there are given for the case $f_{ac} = 1088$ Hz (if not stated otherwise). However, the final receptivity functions are given in § 7.1 for all three examined frequencies.

3. Numerical simulation approach

Direct numerical simulations were performed for the same test case, especially for the same boundary-layer conditions at the position of the vibrator. Because the experiment was performed on an airfoil, upstream and downstream of the roughness/vibrator the parameters in the simulation deviated from those in the experiment. Nevertheless, because of the localized character of the problem studied, this approach is adequate.

The DNS are based on the vorticity–velocity formulation of the complete Navier–Stokes equations using a uniformly spaced grid, fourth-order-accurate finite differences

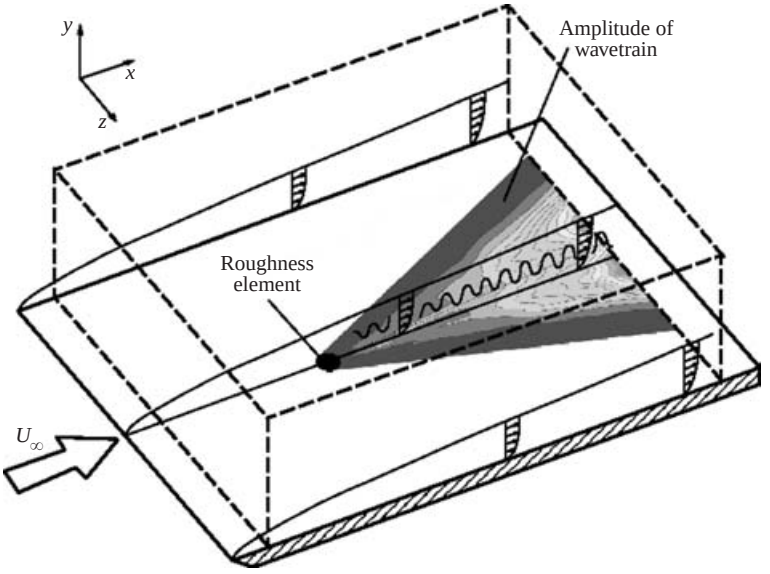

FIGURE 7. Sketch of the integration domain used in the direct numerical simulations.

in the streamwise and wall-normal direction and a spectral representation in the spanwise direction (see Rist & Fasel 1995). In contrast to Rist & Fasel (1995) a 'total variable formulation' is used instead of a 'disturbance variable formulation'. The computational domain is shown in figure 7.

For the present investigations, the sound wave in the free stream is prescribed at inflow as a solution of the second Stokes' problem for a given frequency and amplitude. For the modelling of the surface roughness, a novel wall model has been implemented and compared with standard first-order formulations that consider only a no-slip condition in wall-parallel directions. The use of a body-fitted coordinate system is avoided and the typically small surface roughness is modelled by non-zero velocity at the lowest row of grid points, which are extrapolated from the field in such a way as to fulfil the no-slip condition on the surface of the roughness. Here, this is done using fifth-order polynomials, which are consistent with the finite-difference representation of the flow field. The main difference between the new model and models found in literature is that it takes into account the no-slip condition for the wall-normal velocity on the roughness as well. Thus, at least for larger heights of the surface roughness, this novel formulation should lead to more accurate results, because there is no linearization in it.

The calculation of the complex receptivity function for the interaction of a sound wave of a given frequency with a roughness with a discrete spanwise wavenumber and a certain shape in the streamwise direction requires four numerical simulations (see Wörner *et al.* 2000). In the first simulation, the steady flow over a flat plate with a roughness located at a certain distance from the leading edge is calculated using the unsteady Navier–Stokes equations starting with the flow over a flat plate without roughness. In the second simulation, the interaction of the sound wave with the roughness is calculated using the previously calculated steady flow over the roughness as the initial condition.

The difficulty now is to extract the TS-wave, which is created by the interaction of the sound wave with the roughness, from the total solution. There are two problems.

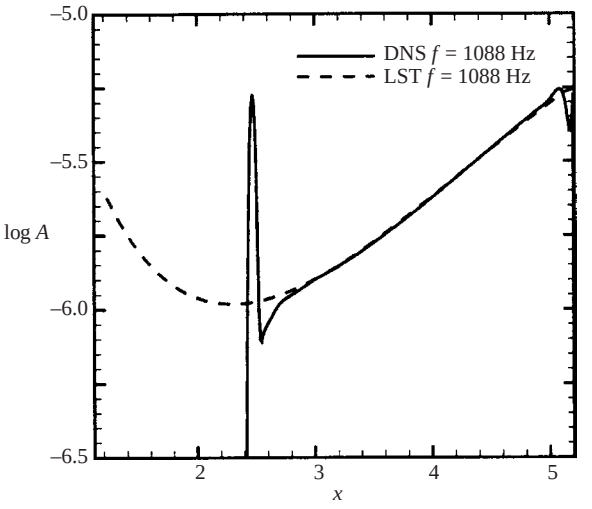

FIGURE 8. Downstream amplitude development of the two-dimensional TS-wave generated at the roughness in comparison to linear stability theory, zero pressure gradient, position of the roughness at $x = 2.471$, $F = 79.1 \times 10^{-6}$.

The first is that the sound wave itself has the same frequency as the created TS-wave and the second is that there is a numerically created TS-wave at the inflow boundary resulting from an inflow boundary condition that is not absolutely correct. This problem is solved using a method suggested by Crouch & Spalart (1995). Therefore, a third simulation is required including the sound wave, but no roughness. In this simulation, the TS-wave created at the inflow boundary is also present. So the TS-wave created at the roughness can be extracted from the total solution by subtracting the results of the third simulation from the results of the second. Then, a Fourier analysis is used to determine the amplitude and phase of the TS-wave at every streamwise position.

In a two-dimensional simulation, a single TS-wave can be observed downstream of the surface roughness. Figure 8 shows the amplitude development of the created disturbance versus the non-dimensional streamwise coordinate x, whereas figure 9 depicts the u-velocity disturbance profile versus y at a location downstream of the surface non-uniformity. The amplification rates, as well as the shape of the $u'(y)$-profile, agree well with those predicted by linear stability theory.

Because of the influence of the near field (see figure 8), the calculated amplitude of the TS-wave at the centre of the roughness element must be extrapolated from the downstream behaviour (similar to the experimental case). This is done by matching the amplitudes of the TS-wave created owing to receptivity at the roughness with the amplitudes of a TS-wave calculated in a fourth simulation by pure blowing and suction at the wall upstream of the roughness element. The behaviour of both TS-waves must be similar downstream of the roughness. So the results of the fourth simulation can be used for the extrapolation.

To check the validity of the code for two-dimensional receptivity simulations, test calculations were performed varying the frequency of the sound wave and the location of the surface non-uniformity relative to the leading edge. The results were compared with results obtained by Choudhari & Streett (1992) with 'finite-Reynolds-number-theory' including a first-order model of the roughness. Choudhari & Streett introduced

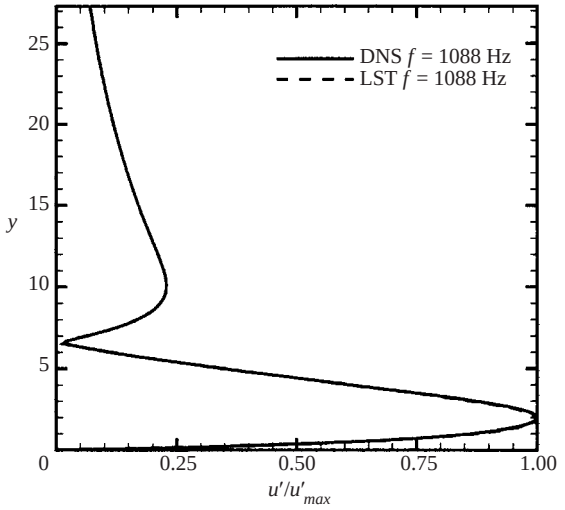

FIGURE 9. Comparison of the two-dimensional TS-eigenfunction calculated for a position downstream of the roughness, $x = 3.27$, $F = 79.1 \times 10^{-6}$.

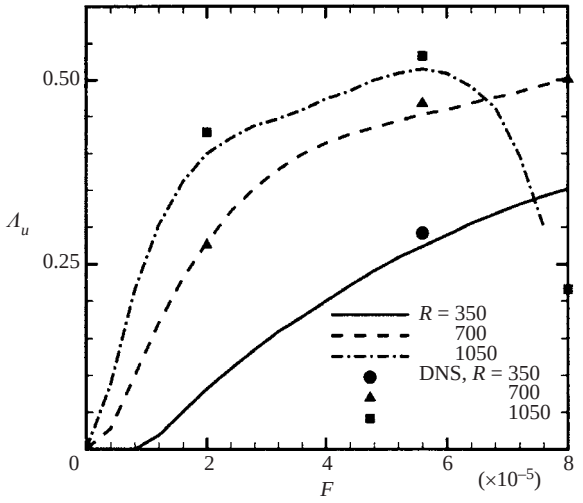

FIGURE 10. Magnitude of the efficiency function (Choudhari & Streett 1992) versus the non-dimensional frequency parameter $F = 2\pi f \nu / U_\infty^2$.

the so-called 'efficiency function' Λ_u that is proportional to the receptivity function (2.7).

For small enough roughness, the DNS with the novel high-order wall model should lead to the same results as the linearized theory by Choudhari & Streett (1992). Figure 10 shows a comparison of the 'efficiency function' for the Blasius boundary layer with results of the DNS calculations. The problem was studied for three different Reynolds numbers (based on δ_1) and as a function of the acoustic frequency. As can be seen, the results agree very well.

The main calculations were performed for the same three acoustic frequencies as in the experiments and for three discrete spanwise wavenumbers, which correspond

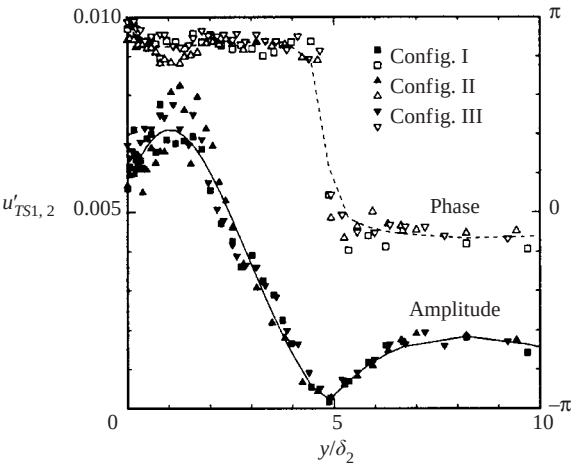

FIGURE 11. Measured normal to wall profiles at the position $s/s_{max} = 0.325$. Config. I: $u'_{ac} = 0.00567\,\mathrm{m\,s^{-1}}$, $A_v = 33\,\mathrm{mm}$; config. II: $u'_{ac} = 0.00249\,\mathrm{m\,s^{-1}}$, $A_v = 33\,\mathrm{mm}$; config. III: $u'_{ac} = 0.00535\,\mathrm{m\,s^{-1}}$, $A_v = 16\,\mathrm{mm}$. The fluctuation amplitude $u'_{TS1,2}$ is normalized by the acoustic and vibrational r.m.s. amplitude and the local free-stream velocity U_δ.

to the TS-wave propagation angles of 0°, 25° and 45°. All other parameters were chosen so that the situation in the DNS represents that in the experiment.

4. Preliminary measurements

This paper focuses on the linear receptivity problem. A criterion for the linearity of the present problem is an independence of the spatial distributions of phases and normalized amplitudes from absolute values of vibrational and acoustic amplitudes. In figure 11, the normal-to-wall profiles of streamwise velocity fluctuations are compared with each other for three different levels of excitation, which cover the whole range of the studied parameters. The fluctuation amplitude $u'_{TS1,2}$ is normalized by the acoustic and vibrational r.m.s. amplitude. All three measurements agree well. In addition the hot-wire signal was checked carefully for the appearance of secondary combination frequencies $f = f_{ac} \pm 2f_v$, the presence of which would indicate the nonlinearity of the receptivity mechanism. To provide the linear development in the wavetrain, which is necessary for the applied method for upstream extrapolation, the acoustic and vibrational forcing was limited so that the maximum r.m.s TS-amplitude at the end of the measurement section was of the order of $u'/U_\delta = 0.02\%$ for the combination frequencies.

During preliminary measurements, it turned out that the acoustic wave excites the membrane of the vibrator at the acoustic frequency. This also leads to very weak membrane oscillations at the combination frequencies $f_{1,2} = f_{ac} \mp f_v$ (probably owing to a weak nonlinearity of the vibrator). These vibrations produce, in turn, TS-waves resulting from the receptivity due to the vibrations themselves. It was found that the possible additional amplitude of the TS-waves excited because of the vibrational receptivity is at least 19 times lower than the amplitude of the TS-waves produced because of the acoustic receptivity.

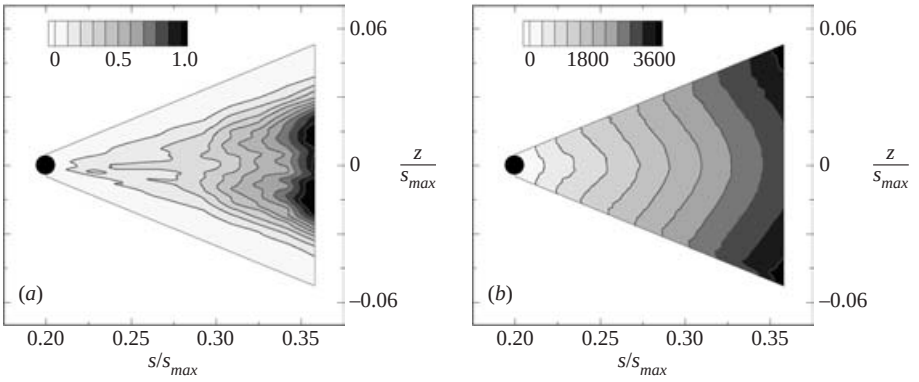

FIGURE 12. (*a*) Downstream development of amplitudes for the 'first' combination mode $f_{TS1} = 1071$ Hz. (*b*) Downstream development of phases for the 'first' combination mode $f_{TS1} = 1071$ Hz.

The quality of the installation of the vibrator with respect to the model surface influences the measurement's signal-to-noise ratio because of additional perturbations entering the boundary layer. These perturbations appear, in particular, due to a scattering of acoustic waves on the edges of the vibrator, which may not be mounted perfectly flush with the wall. This influence was estimated by measuring the transition position, which turned out to be almost at the same streamwise station as for the 'clean' airfoil, including cases when the acoustics or the vibration were switched on.

The orientation of the acoustic wave can be significant for values of the acoustic receptivity coefficients (see Choudhari & Kerschen 1990; Zhou *et al.* 1994). In the experimental situation the high-frequency acoustic wave produced by the loudspeaker inside the wind-tunnel reflected many times from different walls and acoustical non-uniformities. As a result, the acoustic field can have a rather complicated spatial structure, which includes standing waves. Therefore, the angle of inclination of the velocity fluctuation vector with respect to the mean flow was measured with a single slanted hot wire in the (s, z)-plane above the vibrator. This angle was found to be very small, typically below 10°.

5. Downstream evolution of excited TS-waves and their initial spectra

The results of the main hot-wire measurements are illustrated in this section. Prior to the spatial Fourier transform, the measured spanwise distributions were interpolated to an equally spaced grid. The resulting spatial fields of the TS-wave amplitude and phase measured within the wavetrain for the 'first' combination mode $f_1 = f_{ac} - f_v$ ($f_{ac} = 1088$ Hz) are shown in figures 12(*a*) and 12(*b*). Similar fields were obtained for another ('second') combination mode $f_2 = f_{ac} + f_v$, as well as for two other acoustic frequencies studied ($f_{ac} = 720$ and 1562 Hz).

The complex values corresponding to the wavetrain in physical space were mapped for each spanwise scan to the spanwise wavenumber spectra by means of the spatial complex Fourier transform

$$\bar{B}_{TS}(s_i, \beta) = \frac{1}{2\pi} \int_{-\infty}^{\infty} \bar{A}_{TS}(s_i, z) \mathrm{e}^{-\mathrm{i}\beta z} \, \mathrm{d}z.$$

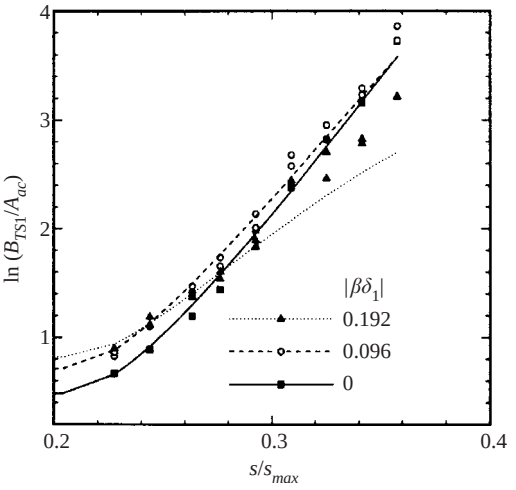

FIGURE 13. Downstream development of amplitudes for three different spanwise wavenumbers in comparison to linear stability theory (lines).

Then, the downstream development of the normal (i.e. harmonic in time and space) oblique waves with different fixed values of the spanwise wavenumber was investigated separately at each fixed combination frequency.

For the determination of the receptivity function (2.1), it was necessary to evaluate the initial complex spectra (amplitudes and phases) of the excited TS-waves, (2.3), at the position of the surface non-uniformity. In previous receptivity experiments, different methods have been used to 'reconstruct' the initial wavenumber spectra of the TS-waves. Ivanov *et al.* (1997) performed an upstream extrapolation of the data by curve fits. Another possibility is to determine these stability characteristics experimentally with a second source placed upstream of the main vibrator (Bake *et al.* 2001). In the present paper, the results from linear stability calculations were used for the extrapolation of the data.

The streamwise development of the normal-mode amplitudes is illustrated in figure 13 for the first combination frequency f_1 (at $f_{ac} = 1088$ Hz) for three different values of the spanwise wavenumber. The wavenumbers shown in figure 13 ($\beta\delta_1 = 0 \pm 0.096$ and ± 0.192) correspond to the propagation angles of 0°, $\pm 26°$ and $\pm 46°$, respectively. The lines denote the amplification curves predicted by the locally parallel linear stability theory, whereas the points correspond to the experimental data. The values obtained at the position of the vibrator centre ($s/s_{max} = 0.2$), with the help of the theoretical amplification curves matched with the experimental points, correspond to the extrapolated initial spectral amplitudes. These values were determined for every fixed spanwise wavenumber β. It can be seen from figure 13 that for high angles (greater than approximately 40°) the locally parallel linear stability theory underestimates the TS-wave increments owing to non-parallel effects (see e.g. Bertolotti 1991; Kachanov, Koptsev & Smorodsky 2000), which are not included in it. In view of this, in order to minimize the extrapolation error, the matching of the theoretical and experimental distributions for high propagation angles was performed only at the beginning of the region of measurements.

The downstream development of the associated phases of the normal TS-modes is shown in figure 14. It can be seen that every set of points is very well fitted by

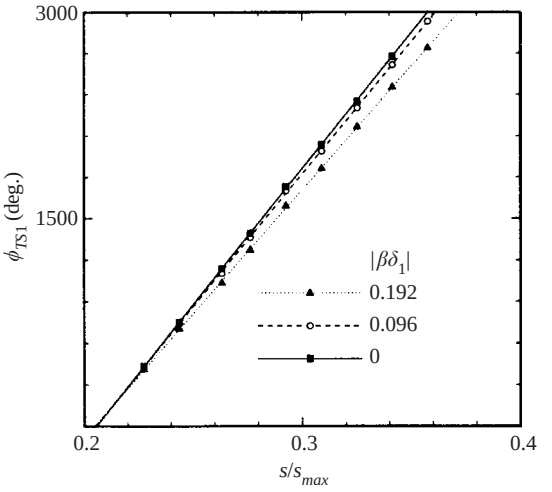

FIGURE 14. Downstream development of phases corresponding to three different spanwise wavenumbers. Lines give linear curve fit.

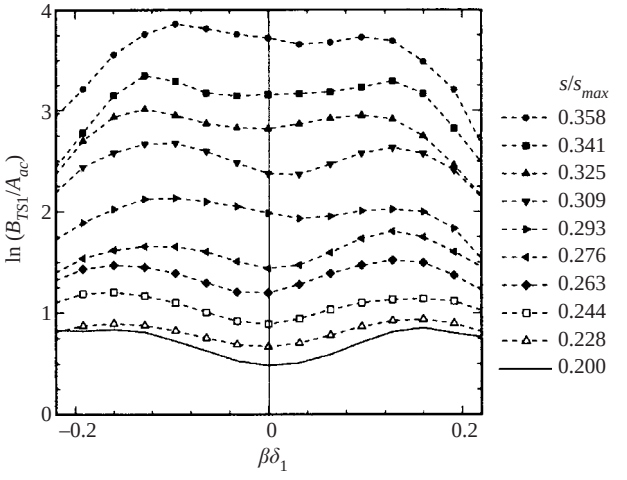

FIGURE 15. - - -, Downstream development of amplitudes in the wavenumber–amplitude plane. The extrapolated initial spectrum at the position of the vibrator.

a straight line, which was used for the extrapolation of the phases to the vibrator centre position. The gradient of each streamwise phase distribution corresponds to the dimensional streamwise wavenumber α_r of the excited TS-wave.

The measured and extrapolated (initial) amplitude parts of the TS-wave spanwise-wavenumber spectra are shown in figure 15 for the first combination frequency f_1 (at $f_{ac} = 1088$ Hz).

6. Resonant spectra of vibrations

Figure 16 shows the dispersion characteristic for the position of the source for two combination frequencies at $f_{ac} = 1088$ Hz. Two kinds of dispersion characteristics are shown in this figure: (i) the streamwise wavenumber versus the spanwise wavenumber

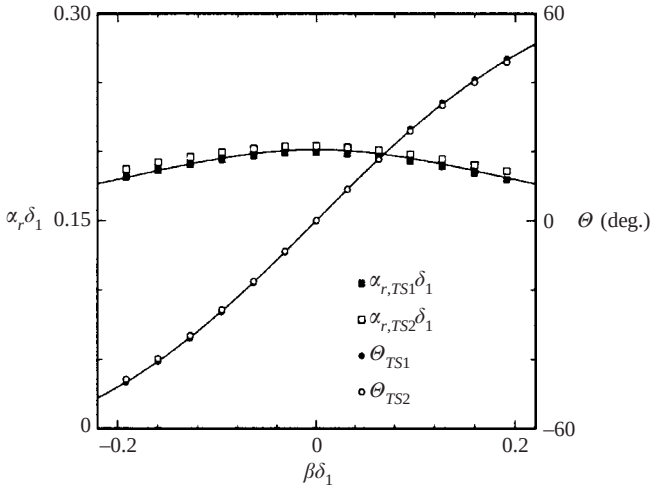

FIGURE 16. Comparison of extrapolated measured (symbols) and calculated (LST, lines) dispersion characteristic at the position of the vibrator.

and (ii) the wave propagation angle versus the spanwise wavenumber. Symbols correspond to the experimental data obtained from the streamwise phase distributions such as those presented in figure 14. The solid lines show for comparison the corresponding dispersion characteristics calculated directly from locally parallel linear stability theory for the same streamwise position. The agreement is remarkably good. Similar results have been obtained for the two other frequencies studied.

The dispersion curves (2.2), like those shown in figure 16, were used for selection of the resonant modes (2.5) in the two-dimensional wavenumber spectrum (2.6) of the shape of the membrane oscillations described above. Only the resonant combination modes discussed in § 2.4 can produce TS-waves in the boundary layer.

The shape of the membrane oscillations was carefully measured (see § 2.2) and then double Fourier transformed in the streamwise (s-coordinate) and spanwise (z-coordinate) directions. The amplitude part of the resulting two-dimensional wavenumber spectrum is shown in figure 17. It is nearly axisymmetric and independent of both the disturbance frequency and amplitude. The spectral phases (not shown) are practically constant in the region of the main cupola of the amplitude spectrum.

From this spectrum, the components of the resonant spectrum (2.5) were selected (line in figure 17) by means of linear interpolation along the line in the $(\alpha_r\delta_1, \beta\delta_1)$-plane, which corresponds to the dispersion function (2.2) (see figure 16). The solid line in figure 17 shows the range of spanwise wavenumbers used during the experimental data processing. This resonant spectrum was used for determination of the receptivity function according to (2.1). (Note that for the very low vibrational frequency used in the present experiment, the resonant spectra for the first and second combination modes merge practically with each other in figure 17.)

7. Receptivity coefficients and their comparison with previous results

7.1. *Receptivity functions in the present experiment and DNS*

Finally, the values of the amplitude and phase parts of the complex receptivity functions were obtained according to definitions (2.1) and (2.7) for the experiment

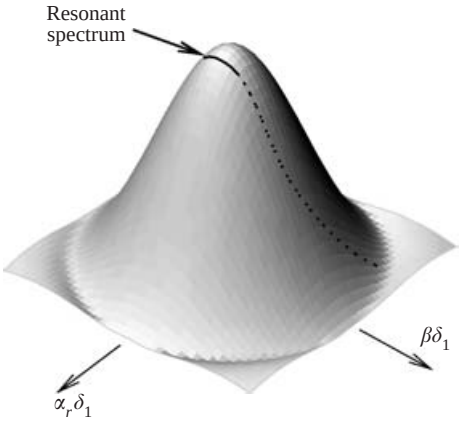

FIGURE 17. Amplitude part of the wavenumber spectrum of the vibrator membrane displacement. The line shows the resonant modes ($f_{ac} = 1088$ Hz) interpolated with the help of the dispersion characteristic, the solid line depicts the part used in the range of the processed wavenumbers.

and DNS, respectively. By means of the dispersion characteristics $\theta_{1,2} = \theta_{1,2}(\beta) = \tan^{-1}(\beta/\tilde{\alpha}_{r1,2})$ obtained for every fixed TS-wave frequency (see figure 16), it is convenient to present the receptivity functions in dependence of the TS-wave propagation angle θ. The results are shown in figures 18(a)–18(c) for $f_{ac} = 720$, 1088 and 1562 Hz, respectively. In the experiment, the receptivity functions are obtained for two combination frequencies in the range of wave propagation angles from $-50°$ to $+50°$.

First of all, figure 18 shows that the amplitude and phase parts of the complex receptivity function, calculated with DNS (large symbols), show very good agreement with those obtained in the experiment. The deviations do not exceed the experimental accuracy estimated from the scattering of the experimental points in different sets of measurements.

As was mentioned in § 2.3, the values for the receptivity functions presented in figure 18 (for both the experiment and DNS) are obtained for a non-dimensional wall distance $y/\delta_2 = 2.2$. For $f_{ac} = 720$ Hz and $f_{ac} = 1088$ Hz, this distance coincides quite well with the position of the maximum amplitude for the TS-eigenfunctions for the studied propagation angles. However, for $f_{ac} = 1562$ Hz, the position of the maximum for the two-dimensional eigenfunction is slightly closer to the wall and, therefore, below the selected y-distance. This leads to somewhat lower values of the receptivity amplitudes for propagation angles $|\theta| \leqslant 10°$.

To clarify this point, figure 19 shows the receptivity amplitudes calculated in DNS for the y-distance used in the measurements (solid lines, black symbols) and for the distances, which correspond to exact (calculated) positions of the TS-amplitude maxima (dashed lines, open symbols). It can be seen that for the two-dimensional-wave ($\theta = 0°$) at $f_{ac} = 1562$ Hz, the receptivity amplitude determined for the experimental distances is about 10% lower than that for the exact maximum position. Because of this, the values of the receptivity amplitude *measured* for zero propagation angle (figure 18) increase first with frequency and then decay for $f_{ac} = 1562$ Hz. However, if we take the influence of the two-dimensional maximum offset into account (figure 19), the two-dimensional receptivity turns out to rise slightly with frequency.

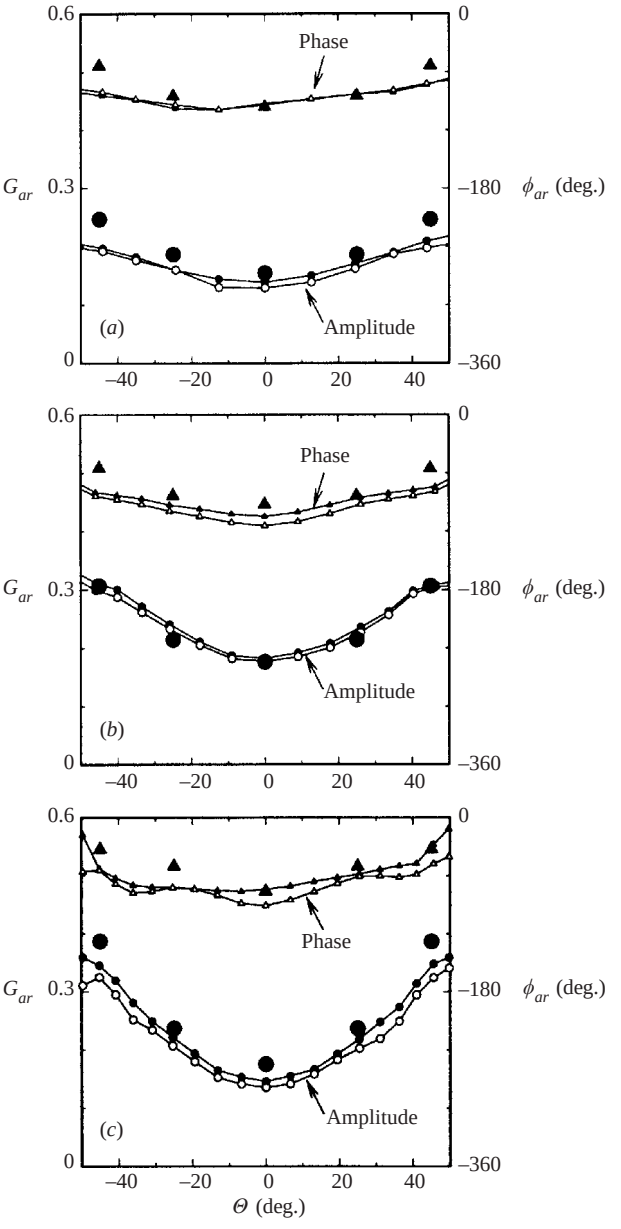

FIGURE 18. (*a*) $f_{ac} = 720\,\text{Hz}$, (*b*) $f_{ac} = 1088\,\text{Hz}$ and (*c*) $f_{ac} = 1562\,\text{Hz}$. The amplitude and phase part of the receptivity function for f_{ac}, solid symbols mark the first, hollow symbols the second combination frequency. Large symbols show results from DNS.

It is seen from figure 18 that, for all studied frequencies, the receptivity is lowest for the two-dimensional case and increases with increasing wave-propagation angle. For $f_{ac} = 720\,\text{Hz}$, this increase is relatively small and reaches a 1.5 times higher value for a 50° propagation angle in comparison with the two-dimensional wave. For the frequency $f_{ac} = 1562\,\text{Hz}$, the receptivity for $\theta = 50°$ is a factor of 2.5 higher in comparison with zero propagation angle. This observation is especially important

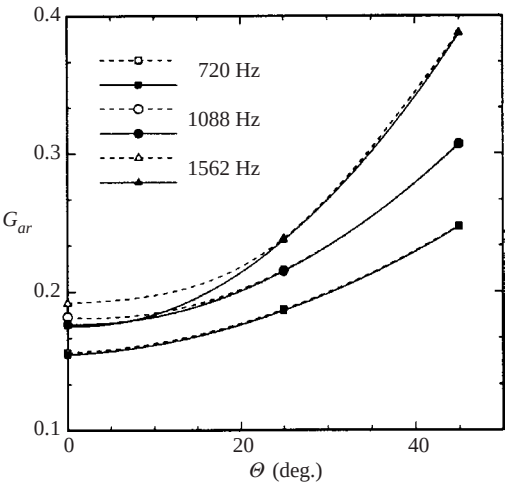

FIGURE 19. Amplitude part of the receptivity function for the investigated frequencies as a function of the propagation angle. DNS results, ---, wall distance corresponding to the maximum of the TS-eigenfunction, —, amplitude corresponding to the y-distance used in the measurements.

for transition in two-dimensional subsonic boundary layers (see § 1). For practically relevant cases, the two-dimensional TS-waves usually reach higher amplitudes, compared to the three-dimensional ones, in the linear stage of the transition development because of the selective stability characteristics of the boundary layer. However, the rather strong angular dependence of the acoustic-roughness receptivity mechanism found in the present study is able to produce a significantly higher initial level of three-dimensional disturbances, which can have an essential influence when entering the nonlinear stage of transition (see e.g. Klebanoff *et al.* 1962; Herbert 1988).

The phase part of the receptivity function is only weakly dependent on the TS-wave propagation angle and frequency, both in experiment and DNS. For the two-dimensional case, the receptivity phase is close to -90° and increases slightly to approximately -45° for propagation angles of $\theta = 50^\circ$.

7.2. *Comparison with related receptivity experiments*

A quantitative comparison with published experimental data can be done for the zero propagation angle only. Saric *et al.* (1991) performed experiments in a Blasius flow for scattering of a plane acoustic wave with non-dimensional frequency of $F = 50 \times 10^{-6}$ on the roughness positioned at $Re_{\delta 1} = 1248$. The results are given as u'_{TS}/u'_{ac} (a kind of receptivity coefficient for fixed roughness shape and height) at the measurement position. In order to compare these values with the receptivity coefficients found in the present work, it is necessary to make some assumptions and to perform additional calculations. The initial (i.e. at the roughness location) amplitude u'_{inTS} of the excited TS-wave can be estimated with the help of an upstream extrapolation by means of linear stability theory. The amplitude of the resonant spectral component $\tilde{C}_r = \tilde{C}_r(\tilde{\alpha}_r)$ of the streamwise-wavenumber spectrum of the roughness element $C_r = C_r(\alpha_r)$ must be determined for the value of the streamwise wavenumber $\tilde{\alpha}_r$, for zero propagation angle. Finally, the coefficient u'_{TS}/u'_{ac}

measured by Saric *et al.* (1991) must be multiplied by u'_{inTS}/u'_{TS} and divided by $\tilde{C}_r(\tilde{\alpha}_r)$. After these transformations, the coefficient can be used directly for comparison. The resulting receptivity coefficient turned out to be $G_{ar} = 0.165$, that is somewhat higher than $G_{ar} = 0.134$, obtained in the present work for a non-dimensional frequency of $F = 52.4 \times 10^{-6}$ and a local Reynolds number of $Re_{\delta 1} = 805$. To compare finally the receptivity coefficients for equal conditions, the influence of the Reynolds number and frequency parameter was estimated with the help of the theoretical results by Choudhari & Streett (1992) (cf. figure 10). Applied to the receptivity coefficient of Saric *et al.* (1991), this leads to $G_{ar} = 0.124$, which is now fairly close to the present value.

A similar comparison can be performed with experiments by Kosorygin *et al.* (1995). In this case, the non-dimensional frequency had a value of $F = 32.7 \times 10^{-6}$ and the rectangular roughness was positioned at $Re_{\delta 1} = 1509$. The receptivity coefficient was defined in that paper as $K_s = u'_{TS,I}/u'_{ac,I}$, where $u'_{TS,I}$, $u'_{ac,I}$ are the r.m.s. amplitudes of the two-dimensional TS-wave and the acoustic wave, respectively, determined at the position of the first branch of the neutral stability curve (which coincides with the position of the roughness). It was found that $K_s = 0.031$. After normalization with $\tilde{C}_r(\tilde{\alpha}_r)$ (see above) this gives a receptivity coefficient for the experiments by Kosorygin *et al.* (1995) of $G_{ar} = 0.212$. Taking again the influence of Reynolds number and frequency parameter into account, which requires an interpolation over a wider range than for the experiment of Saric *et al.* (1991), this value reduces to $G_{ar} = 0.161$ for the present conditions and becomes rather close to (somewhat higher than) the value of $G_{ar} = 0.134$ reported here.

The results obtained in the present study on three-dimensional acoustic-roughness receptivity can also be compared qualitatively with the *vibrational receptivity problem*, which was studied by Ivanov *et al.* (1998*b*) and Bake *et al.* (2001) for the Blasius boundary layer. In the case of acoustic receptivity, the TS-wave is excited owing to scattering of the large-wavelength acoustic wave on a short-scale, localized surface roughness. Meanwhile, in the case of vibrational receptivity the TS-wave is excited directly by the surface vibrations, which contain spatial scales of the order of the TS-wavelength. One of the non-dimensional frequencies ($F \times 10^{-6} = 81.4$) examined by Ivanov *et al.* (1998*b*) is close to one of those studied in the present experiment ($F \times 10^{-6} = 79.1$); the local Reynolds number ($Re_{\delta 1} = 739$) at the position of the source is also similar ($Re_{\delta 1} = 805$). In addition, a complete Fourier decomposition was performed in that work and the receptivity functions were evaluated as the ratio of the complex initial wavenumber spectrum of excited TS-waves and the resonant complex spectrum of the surface vibrations. Owing to the absence of acoustic forcing, this definition of the receptivity function is, of course, different from (2.1). However, it is possible to compare the receptivity functions obtained in these two cases if we multiply the acoustic-roughness coefficients by a fixed amplitude of the acoustic forcing. This reduces (2.1) to the same definition as was used in the study of vibrational receptivity. By introducing a level of 116.2 dB ($u'_{ac} = 0.032\,\mathrm{m\,s^{-1}}$) for the acoustics, the receptivity amplitudes become approximately the same (for a propagation angle of 35°) as those for the vibrational receptivity (figure 20). For higher levels of the acoustic amplitude, the acoustic-roughness receptivity generates higher initial TS-waves, for the same equivalent roughness height, than the vibrational receptivity mechanism. The receptivity phases were processed in a similar way by adding a constant offset ($\Delta\phi = 204°$) to fit both curves for 35° propagation angle.

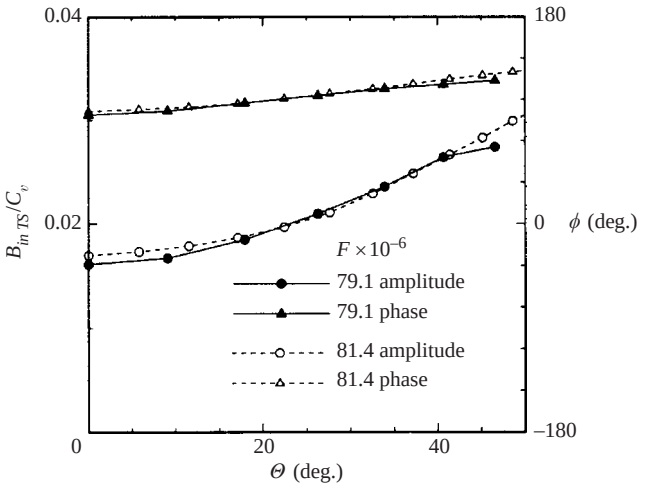

FIGURE 20. —, Comparison of acoustic-roughness receptivity to - - -, vibrational receptivity. To match the curves for 35° propagation angle the acoustic-roughness coefficients are multiplied with a fixed acoustic amplitude of 116.2 dB and the corresponding phases are shifted by an offset of 204°.

Figure 20 shows the results for the frequency parameter investigated. It is apparent that the same angular dependence is found for both receptivity mechanisms, for the amplitudes as well as for the phases. The small difference in the amplitude part for propagation angles less than 20° can be explained by the slightly different wall distances used in both experiments for the measurement of the TS-wavetrains. The consistency of the angular dependence of the receptivity coefficients for the present case, the three-dimensional acoustic-roughness receptivity, and the three-dimensional vibrational receptivity studied by Ivanov *et al.* (1998*b*) gives reason to the assumption that the two mechanisms have a substantial similarity in their physical natures.

8. Conclusions

The results of the present study can be summarized briefly in the following way. The linear three-dimensional acoustic receptivity due to localized quasi-stationary surface non-uniformities has been studied experimentally and numerically for three different acoustic frequencies in a range, which corresponds to the most amplified TS-waves. The quantitative measurements were performed in a laminar two-dimensional subsonic boundary layer of a symmetric airfoil section at zero angle of attack.

In the experiment, the surface non-uniformity was modelled by a circular membrane vibrating at a very low frequency compared to the acoustic one. Under the conditions of a strictly phase-locked measurement, this made it possible to separate the TS-wave in the hot-wire signal from the acoustic wave and associated vibrations by means of Fourier analysis (similar to experiments by Ivanov *et al.* 1997). In the DNS, the surface non-uniformity was steady. The streamwise position of the surface non-uniformity was chosen close to the first branch of the neutral stability curve (for two-dimensional perturbations). In the experiment, the boundary-layer profile at this point was very

close to the Blasius one. Therefore, the accompanying DNS have been performed for the Blasius flow. The DNS are based on the vorticity–velocity formulation of the complete Navier–Stokes equations using a uniformly spaced grid in the streamwise and wall-normal direction and a spectral representation in the spanwise direction. The sound wave in the free stream was prescribed as a solution of the second Stokes' problem at inflow. A novel wall model was implemented in the DNS, which avoids the use of a body-fitted coordinate system and linearization.

A complete complex Fourier decomposition of the involved TS-disturbances and the shape of the surface non-uniformity was performed to map the data from physical space onto the corresponding Fourier space (frequency–wavenumber). The development of the normal Fourier mode amplitudes in the TS-wavetrain showed a good agreement to the locally parallel linear stability theory. This stability theory was used in the experiment for the upstream extrapolation of the normal TS-mode amplitudes from the region of the hot-wire measurements to the surface non-uniformity. The resonant spectral modes were selected from the two-dimensional wavenumber spectrum of the measured shape of the surface non-uniformity along the dispersion curve. Those values were used (together with the involved acoustic amplitudes and phases) to determine the acoustic-roughness receptivity coefficients as functions of the TS-wave frequency and propagation angle.

The comparison of the experimental receptivity amplitudes and phases with those obtained in the accompanying DNS has shown a very good agreement in the range of parameters studied. Taking into account that the quantitative determination of the receptivity function represents very extensive data processing, which includes the data approximations and extrapolations, the present combined experimental and DNS study is the most reliable way to ensure high-quality results.

One of the main results is that the acoustic-roughness receptivity mechanism generates three-dimensional waves much more effectively (up to 2.5 times in the range of parameters studied) than two-dimensional ones. The acoustic-roughness receptivity amplitudes are found to increase with acoustic wave frequency for all propagation angles. The most significant frequency dependence is observed again for three-dimensional modes inclined at large angles to the flow direction. The predominance of the three-dimensional acoustic-roughness receptivity mechanism is of importance for practically relevant cases, because the three-dimensional TS-waves play a very significant role at nonlinear stages of transition (see e.g. Klebanoff *et al.* 1962; Herbert 1988).

In contrast to the receptivity amplitudes, the corresponding phases depend only weakly on the frequency and spanwise wavenumber.

The results obtained in the present paper for the acoustic-roughness receptivity exhibit features which are very similar to those observed for pure vibrational receptivity (Ivanov *et al.* 1998*b*), mainly a significant angular dependence of the receptivity amplitudes and a rather weak change in the corresponding phases.

As previous experimental results were obtained solely for the two-dimensional case, a quantitative comparison of the three-dimensional acoustic-roughness receptivity characteristics studied in the present work can only be performed for the particular case of zero spanwise wavenumber. A good overall consistency is found with measurements by Saric *et al.* (1991) and Kosorygin *et al.* (1995).

Owing to the complete Fourier decomposition of all perturbations in the present work, the determined receptivity functions are independent of the specific physical shape of the surface non-uniformity and the results can be used directly for validation of linear receptivity theories.

This work was performed under a grant of the German Research Council (DFG) and is a part of the research program 'Transition'. The contribution of Y. S. Kachanov was supported by SEW-Eurodrive and Volkswagen Stiftung.

REFERENCES

Aizin, L. B. & Polyakov, N. F. 1979 Acoustic generation of Tollmien–Schlichting waves over local unevenness of surface immersed in stream. *Preprint No 17. USSR Acad. Sci. Sib. Div. Inst. Theor. Appl. Mech. Novosibirsk* (in Russian).

Bake, S., Ivanov, A. V., Fernholz, H. H., Neemann, K. & Kachanov, Y. S. 2001 Receptivity of boundary layers to three-dimensional disturbances. *Eur. J. Mech.* B *Fluids* **21**, 29–48.

Bertolotti, F. P. 1991 Linear and nonlinear stability of boundary layers with streamwise varying properties. PhD dissertation, Ohio State University, USA.

Cebeci, T., Smith, A. M. O. 1974 *Analysis of Turbulent Boundary Layers*. Academic.

Choudhari, M. 1994 Roughness-induced generation of crossflow vortices in three-dimensional boundary layers. *Theoret. Comput. Fluid Dyn.* **6**, 1–30.

Choudhari, M. & Kerschen, E. J. 1990 Instability wave patterns generated by interaction of sound wave with three-dimensional wall suction or roughness. *AIAA Paper* 90-0119.

Choudhari, M. & Streett, C. L. 1992 A finite Reynolds number approach for the prediction of boundary-layer receptivity in localized regions. *Phys. Fluids* A **4**, 2495–2514.

Conte, S. D. 1966 The numerical solution of linear boundary value problems. *SIAM Rev.* **8**, 3.

Crouch, J. D. 1992 Localized receptivity of boundary layers. *Phys. Fluids* A **4**, 1408–1414.

Crouch, J. D. 1993 Receptivity of three-dimensional boundary layers. *AIAA Paper* 93-0074.

Crouch, J. D. 1994 Theoretical studies on the receptivity of boundary layers. *AIAA Paper* 94-2224.

Crouch, J. D. & Spalart, P. R. 1995 A study of non-parallel and nonlinear effects on the localized receptivity of boundary layers. *J. Fluid Mech.* **290**, 29–37.

Cullen, L. M. & Horton, H. P. 1999 Acoustic receptivity in boundary layers with surface roughness. In *Laminar–Turbulent Transition* (ed. H. Fasel & W. Saric), pp. 43–50. IUTAM Symposium, Sedona, AZ, USA.

Drela, M. & Giles, M. B. 1986 Viscous–inviscid analysis of transonic and low Reynolds number airfoils. *AIAA*-86-1786-CP.

Fyodorov, A. V. 1988 Excitation of cross-flow instability waves in boundary layer on a swept-wing. *Zhurn. Prikl. Mekhan. Tekhn. Fiz.* **5**, 46–52 (in Russian).

Gaponenko, V. R., Ivanov, A. V. & Kachanov, Y. S. 1996 Experimental study of three-dimensional boundary-layer receptivity to surface vibrations. In *Nonlinear Instability and Transition in Three-Dimensional Boundary Layers* (ed. P. W. Duck & P. Hall), pp. 389–398. Kluwer.

Gaster, M. 1965 On the generation of spatially growing waves in a boundary layer. *J. Fluid Mech.* **22**, 433–441.

Gilyov, V. M. & Kozlov, V. V. 1984 Excitation of Tollmien–Schlichting waves in a boundary layer on a vibrating surface. *Zhurn. Prikl. Mekhan. Tekhn. Fiz.* **6**, 73–77 (in Russian).

Goldstein, M. E. 1985 Scattering of acoustic waves into Tollmien–Schlichting waves by small streamwise variation in surface geometry. *J. Fluid Mech.* **154**, 509–529.

Goldstein, M. E. & Hultgren, L. S. 1989 Boundary-layer receptivity to long-wave free-stream disturbances. *Annu. Rev. Fluid Mech.* **21**, 137–166.

Herbert, T. 1988 Secondary instability of boundary layer. *Annu. Rev. Fluid Mech.* **20**, 487–526.

Ivanov, A. V., Kachanov, Y. S. & Koptsev, D. B. 1997 An experimental investigation of instability wave excitation in three-dimensional boundary layer at acoustic wave scattering on a vibrator. *Thermophys. Aeromech.* **4**, 359–372.

Ivanov, A. V., Kachanov, Y. S. & Koptsev, D. B. 1998 Method of phased roughness for determining the acoustic receptivity coefficients. In *9th Intl Conf. Methods of Aerophys. Res. Proc. Part II,* pp. 89–94. Inst. Theor. & Appl. Mech., Novosibirsk.

Ivanov, A. V., Kachanov, Y. S., Obolentseva, T. G. & Michalke, A. 1998*b* Receptivity of the Blasius boundary layer to surface vibrations. Comparison of theory and experiment. In *9th Intl Conf. Methods of Aerophys. Res. Proc. Part I*, pp. 93–98. Inst. Theor. & Appl. Mech., Novosibirsk.

Kachanov, Y. S. 2000 Three-dimensional receptivity of boundary layers. *Eur. J. Mech.* B *Fluids* **19**, 723–744.

Kachanov, Y. S., Koptsev, D. B. & Smorodsky, B. V. 2000. Three-dimensional stability of self-similar boundary layer with a negative Hartree parameter. 2. Characteristics of stability. *Thermophys Aeromech.* **7**, 341–351.

Kachanov, Y. S., Kozlov, V. V. & Levchenko, V. Y. 1975 Generation and development of small disturbances in laminar boundary layer under the action of acoustic fields. *Izv. Sib. Otd. Akad. Nauk USSR, Ser. Tekh. Nauk.* **13**(3), 18–26 (in Russian).

Kachanov, Y. S., Kozlov, V. V. & Levchenko, V. Y. 1978 Origin of Tollmien–Schlichting waves in boundary layer under the influence of external disturbances. *Izv. Akad. Nauk USSR, Mekh. Zhid. i Gaza.* 5, pp. 85–94 (in Russian). (See translation into English in *Fluid Dyn.* **13** (1979) 704–711)

Kachanov, Y. S., Kozlov, V. V. & Levchenko, V. Y. 1982 *Onset of Turbulence in Boundary Layers.* Nauka, Novosibirsk (in Russian).

Kachanov, Y. S., Kozlov, V. V., Levchenko, V. Y. & Maksimov, V. P. 1979 Transformation of external disturbances into the boundary-layer waves. In *Proc. Sixth Intl Conf. on Numerical Methods in Fluid Dyn.* Springer, Berlin, pp. 299–307.

Kachanov, Y. S. & Levchenko, V. Y. 1984 The resonant interaction of disturbances at laminar–turbulent transition in a boundary layer. *J. Fluid Mech.* **138**, 209–247.

Kachanov, Y. S. & Obolentseva, T. G. 1996 A method of study of influence of the flow nonparallelism on the three-dimensional stability of Blasius boundary layer. In *8th Intl Conf. Methods of Aerophys. Res. Proc. Part II*, pp. 100–105, Inst. Theor. & Appl. Mech., Novosibirsk.

Kachanov, Y. S. & Obolentseva, T. G. 1998 Development of three-dimensional disturbances in the Blasius boundary layer. 3. Nonparallelism effects. *Thermophys. Aeromech.* **5**, 331–338.

Kerschen, E. J. 1989 Boundary layer receptivity. *AIAA Paper* 89-1109.

Kerschen, E. J., Choudhari, M. & Heinrich, R. A. 1990 Generation of boundary-layer instability waves by acoustic and vortical free-stream disturbances. In *Laminar–Turbulent Transition* (ed. D. Arnal & R. Michel), pp. 477–484. Springer.

Klebanoff, P. S., Tidstrom, K. D. & Sargent, L. M. 1962 The three-dimensional nature of boundary-layer instability. *J. Fluid Mech.* **12**, 1–34.

Kosorygin, V. S. 1986 Experimental investigation of laminar boundary layer at low natural and acoustic perturbations. Ph.D. thesis, Inst. Theor. & Appl. Mech., Novosibirsk (in Russian).

Kosorygin, V. S., Levchenko, V. Y. & Polyakov, N. F. 1985 On generation and evolution of waves in laminar boundary layer. In *Laminar–Turbulent Transition* (ed. V. V. Kozlov), pp. 233–242. Springer.

Kosorygin, V. V., Radeztsky, R. H. & Saric, W. S. 1995 Laminar boundary-layer sound receptivity and control. In *Laminar–Turbulent Transition* (ed. R. Kobayashi), pp. 417–524. Springer, Berlin.

Kozlov, V. V. & Ryzhov, O. S. 1990 Receptivity of boundary layers: asymptotic theory and experiment. *Proc. R. Soc. Lond.* A **429**, 341–373.

Leehey, P. 1980 Influence of environment in laminar boundary-layer control. In *Viscous Flow Drag Reduction* vol. 72, pp. 4–16, (ed. G. Hough).

Loehrke, R. I., Morkovin, M. V. & Fejer, A. A. 1975 Review – Transition in nonreversing oscillating boundary layer. *Trans. ASME. J. Fluids Engng* **97**, 534–549.

Maksimov, V. P. 1979 Genesis of Tollmien–Schlichting wave in oscillating boundary layers. In *Development of Perturbations in Boundary Layers* (ed. V. Y. Levchenko), pp. 68–75. Inst. Theor. & Appl. Mech., Siberian Div., USSR Acad. Sci. Novosibirsk (in Russian).

Mangur, C. J. 1977 On the sensitivity of shear layers to sound. *AIAA Paper* 77-1369.

Morkovin, M. V. 1968 Critical evaluation of transition flow laminar to turbulent shear layers with emphasis of hypersonically traveling bodies. *AFFDL TR*, 68–149.

Morkovin, M. V. 1977 Instability, transition to turbulence and predictability. *AGARD-AG-* 236.

Morkovin, M. V. & Reshotko, E. 1990 Dialogue on progress and issues in stability and transition research. In *Laminar–Turbulent Transition* (ed. D. Arnal & R. Michel), pp. 3–29. Springer.

Murdock, J. W. 1980 The generation of Tollmien–Schlichting wave by a sound wave. *Proc. R. Soc. Lond.* A **372**, 1517.

Nishioka, M. & Morkovin, M. V. 1986 Boundary-layer receptivity to unsteady pressure gradients: experiments and overview. *J. Fluid Mech.* **171**, 219–261.

Reshotko, E. 1976 Boundary-layer stability and transition. *Annu. Rev. Fluid Mech.* **8**, 311–349.

Rist, U. & Fasel, H. 1995 Direct numerical simulation of controlled transition in a flat-plate boundary layer. *J. Fluid Mech.* **298**, 211–248.

Rogler, H. L. 1977 The coupling between free-stream disturbances driver oscillations, forced oscillations and stability waves in a spatial analysis of a boundary layer. *AGARD Symp. Laminar–Turbulent Transition. AGARD-CP*-244, Paper 16. Copenhagen.

Rogler, H. L. & Reshotko, E. 1975 Disturbances in a boundary layer introduced by a low intensity array of vortices. *SIAM J. Appl. Mech.* **28**, 431–462.

Ruban, A. I. 1985 On the generation of Tollmien–Schlichting waves by sound. *Fluid Dyn.* **19**, 709–716.

Saric, W. S., Hoos, J. A. & Kohama, Y. 1990 Boundary-layer receptivity: part 1: Freestream sound and two-dimensional roughness strips. *Report, CEAS-CR-R-90191*, Arizona State University, College of Engineering and Applied Sciences, Tempe.

Saric, W., Hoos, J. A. & Radeztsky, R. H. 1991 Boundary layer receptivity of sound with roughness. In *Boundary Layer Stability and Transition to Turbulence* (ed. D. C. Reda, H. L. Reed & R. Kobayashi) vol. 114, pp. 17–22. *ASME-FED*, New York.

Saric W. S., Kozlov, V. V. & Levchenko, V. Y. 1984 Forced and unforced subharmonic resonance in boundary-layer transition. *AIAA Paper* 84-0007.

Schubauer, G. B. & Skramstad, H. K. 1947 Laminar boundary-layer oscillations and transition on a flat plate. *J. Res. Natl Bur. Stand.* **38**1, 251–292.

Squire, H. D. 1933 On the stability for three-dimensional disturbances of viscous fluid between parallel walls. *Proc. R. Soc. Lond.* A **142**, 621–628.

Tadjfar, M. 1990 Receptivity of laminar boundary layer to the interaction of a three dimensional roughness element with time-harmonic free-stream disturbances. PhD dissertation, Dept. Aero. & Astro. Engng, Ohio State University.

Tadjfar, M. & Bodonyi, R. J. 1992 Receptivity of laminar boundary layer to the interaction of a three dimensional roughness element with time-harmonic free-stream disturbances. *J. Fluid Mech.* **242**, 701–720.

Tam, C. K. W. 1978 Excitation of instability waves in a two-dimensional shear layer by sound. *J. Fluid Mech.* **89**, 357–371.

Terent'ev, E. D. 1981 A linear problem on a vibrator in subsonic boundary layer. *Prikl. Matem. Mekhan.* **45**, 1049–1055 (in Russian).

Wiegel, M. & Wlezien, R. W. 1993 Acoustic receptivity of laminar boundary layers over wavy walls. *AIAA Paper* 93-3280.

Wörner, A., Rist, U., Herr, S., Würz, W., Wagner, S. & Kachanov, Y. S. 2000 Study of the acoustic receptivity of a Blasius boundary layer in the presence of a surface non-uniformity. CD-ROM Proc. ECCOMAS 2000, 11–14 September 2000, Barcelona, pp. 1–9.

Wortmann, F. X. & Althaus, D. 1964 Der Laminarwindkanal des Instituts für Aerodynamik und Gasdynamik der Technischen Hochschule Stuttgart. *Z. Flugwiss* **12**, 4.

Würz, W. 1995 Hitzdrahtmessungen zum laminar-turbulenten Strömungsumschlag in anliegenden Grenzschichten und Ablöseblasen sowie Vergleich mit der linearen Stabilitätstheorie und empirischen Umschlagskriterien. Dissertation, Institut für Aero- und Gasdynamik der Universität Stuttgart.

Würz, W., Herr, S., Wagner, S. & Kachanov, Y. S. 1998 Experimental investigations on three-dimensional acoustic receptivity of a laminar boundary layer in the presence of surface non-uniformities. 11. DGLR/AG-STAB Fach-Symposium, Berlin, 10–12.11.1998. In *New Results in Numerical and Experimental Fluid Mechanics* (ed. W. Nitsche, H. J. Heinemann & H. Hilbig) NNFM, vol. 72, Vielweg, Wiesbaden.

Würz, W., Herr, S., Wörner, A., Rist, U., Wagner, S. & Kachanov, Y. S. 1999 Study of three-dimensional wall roughness acoustic receptivity on an airfoil. In *Laminar–Turbulent Transition* (ed. H. Fasel & W. Saric), IUTAM Symposium, Sedona, AZ, USA, 91–96.

Zavol'skii, N. A., Reutov, V. P. & Rybushkina, G. V. 1983 Generation of Tollmien–Schlichting waves via scattering of acoustic and vortex perturbations in boundary layer on a wavy surface. *J. Appl. Mech. Tech. Phys.* **24**, 355–361.

Zhigulyov, V. N. & Tumin, A. M. 1987 *Origin of Turbulence*. Nauka, Novosibirsk (in Russian).

Zhou, M. D., Liu, D. P. & Blackwelder, R. F. 1994 An experimental study of receptivity of acoustic waves in laminar boundary layers. *Exps. Fluids* **17**, 1–9.